View metadata, citation and similar papers at core.ac.uk
brought to you by CORE
provided by University of Southern Queensland ePrints

Sub-domain scaling for finite element analysis of electrical machines

A.J. Hewitt and A. Ahfock

Abstract: Finite element modelling of geometries with large dimensional differences between adjacent sub-domains or domains which have poor aspect ratios can impose significant demands on meshing algorithms and computational resources. A simple sub-domain scaling technique for electromagnetic analysis of electrical machines by finite element analysis is proposed. The technique can be used to improve aspect ratios and is useful in modelling electrical machines with small air gap lengths.

1 Introduction

Finite element analysis is now a well accepted tool for the design and analysis of practically all types of electrical machines [1, 2]. The small air gap length of an electrical machine compared to its other dimensions can, however, make it difficult or even impossible to obtain accurate field solutions [1]. Techniques based on the use of shell elements [3], specialist air-gap elements [4, 5], or the coupling of finite element analysis with an analytical solution [6], have been proposed to overcome this problem. There have also been other techniques [7–10], not specifically related to electrical machines, on geometry transformations and for overcoming meshing difficulties in the finite element method. All of these techniques require some form of modification to the finite element formulation. The method proposed here is based on a rescaling of the air gap region. The original problem, with the narrow air gap, is mapped onto a scaled problem with an improved aspect ratio. Compared to previous techniques, a major advantage of the proposed method is that for axial flux machines, it can be simply implemented using any standard finite element package, as it is independent of the finite element formulation. For radial flux machines, application of the method is equally simple if the finite element software supports position dependence for the material properties.

From the user's viewpoint the technique involves:

(a) choosing a scaling factor (k_a) to expand the original air gap length so that the aspect ratios are sufficiently improved in the scaled problem;

(b) evaluating sub-domain dimensions and material properties for the scaled problem based on the value of k_a and the dimensions and material properties of the original problem;

(c) determining the field solutions to the scaled problem using a finite element package; and

(d) transforming the field solutions obtained for the scaled equivalent problem into solutions for the original problem.

© IEE, 2005

IEE Proceedings online no. 20055078

doi:10.1049/ip-epa:20055078

Paper first received 29th June and in revised form 28th October 2004. Originally published online: 24th January 2005

The authors are with the FOES, Faculty of Engineering, University of Southern Queensland, Toowoombu, Queensland 4350, Australia

The objectives of this paper are:

- to illustrate the benefit of improved aspect ratios;
- to derive the transformation rules that permit a user to transform the original problem into an equivalent scaled problem;
- to derive the rules for transforming the field solutions to the scaled problem into the field solutions to the original problem;
- to demonstrate that the transformation rules have the useful property of power invariance; and
- to demonstrate the benefits of using the proposed technique in a practical problem.

2 Finite element analysis

2.1 The finite element mesh

The finite element method (FEM) is based on the discretisation of the domain under consideration. The mesh quality or element aspect ratio can have a significant effect on the solution accuracy [11, 12]. When meshing adjacent sub-domains with large size differences the mesh can become distorted if the number of elements is insufficient. Maintaining good element quality often requires large numbers of elements and their associated nodes. This can be most easily seen in a two-dimensional example. Consider the domain represented in Fig. 1 where a large sub-domain is adjacent to a much smaller one and triangular elements have been chosen. The nodes at the boundary between the two sub-domains are common to the elements on either side and thus the element sizes are comparable near this boundary. Due to the thinness of sub-domain 2 the characteristic size (d) of an element in this region is equal to the region's height. Ideally, the element shape is an equilateral triangle as seen in Fig. 1. This restriction alone requires a significant number of elements to mesh a region

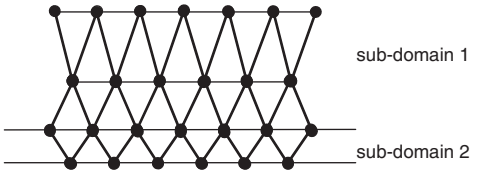

Fig. 1 *Simple mesh across boundary between a small to larger sub-domain*

Authorized licensed use limited to: UNIVERSITY OF SOUTHERN QUEENSLAND. Downloaded on February 25,2010 at 06:40:11 EST from IEEE Xplore. Restrictions apply.

which is thin in one direction and significantly larger in the other. At the boundary, elements of sub-domain 1 have edges of the same lengths as those in sub-domain 2 because of their common nodes. Away from the boundary the elements can grow in size. However, this requires a gradual transition in order to maintain an acceptable element aspect ratio. In these circumstances the number of elements required to mesh the domain rapidly increases as d decreases. Depending on the desired accuracy of the solution in sub-domain 2, the maximum element size may not be desirable which will further exaggerate the problem. This problem is considerably worse when performing three-dimensional meshing on geometries containing sub-domains with poor aspect ratios. The number of nodes/elements determines the computing resources required to solve a finite element problem and thus it is highly desirable to reduce this number whilst retaining desired solution accuracy.

2.2 Quasi-static formulations

There are a number of different quasi-static finite element formulations, two of the more common being the $A-\phi$ (magnetic vector potential – electric scalar potential) and $T-\Omega$ (electric vector potential – magnetic scalar potential) methods. However, all formulations are based on the quasi-static approximation to Maxwell's equations i.e.

$$\nabla \cdot \vec{B} = 0 \tag{1}$$

$$\nabla \times \vec{H} = \vec{J} \tag{2}$$

$$\nabla \times \vec{E} = -\frac{\partial \vec{B}}{\partial t} \tag{3}$$

where $\vec{E}$ is the electric field intensity, $\vec{H}$ is the magnetic field intensity, $\vec{B}$ is the magnetic flux density, $\vec{J}$ is the current density and t is time.

3 Scaling equations

Two scaling strategies with respect to a cylindrical coordinate system have been developed. Scaling in the axial direction is desirable when modelling axial flux machines (AFM) in which the air gap length is defined in the axial (or z) direction. Radial scaling is equivalently attractive when considering radial flux machines (RFM) in which the air gap length is defined along the radial direction.

Consider an RFM structure as three separate regions:

1) the rotor region $0 \leq r \leq r_r$,

2) the air gap region $r_r \leq r \leq r_g$, and

3) the stator region $r_g \leq r \leq r_s$

where r_r is the rotor radius and r_g and r_s are the inner and outer radii of the stator region, respectively. No scaling is required in the rotor region. The air gap region is extended in the radial direction by a factor k_a, so that the unscaled air gap length

$$l_g = (r_g - r_r) \tag{4}$$

becomes

$$k_a l_g = k_a (r_g - r_r) \tag{5}$$

The stator region must now be extended to accommodate the scaled air gap region. A simple linear scaling coefficient (k_s) for the stator region is chosen to permit expansion of the air gap region. Therefore,

$$k_s = \frac{r_r + k_a l_g}{r_r + l_g} \tag{6}$$

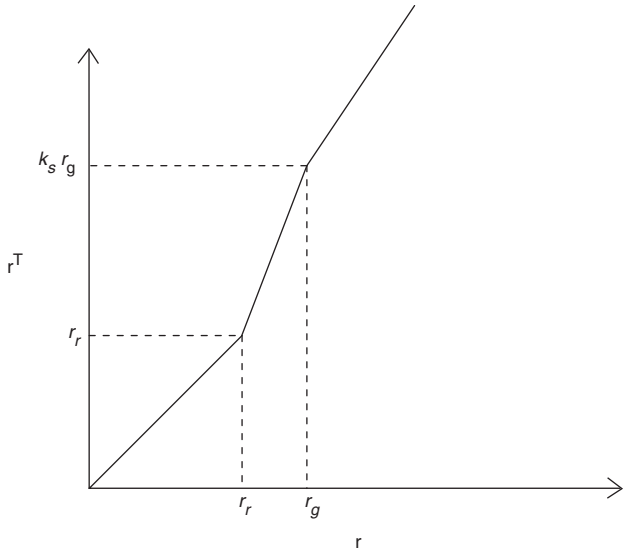

Fig. 2 *Radius mapping from original to the scaled regions*

Figure 2 shows the mapping from the original to the transformed radial coordinate in each of the three regions.

A transformation function $k(r)$ can now be deduced for the air gap region

$$k(r) = \frac{r^T}{r} = \frac{1}{r}\left[\frac{(k_s r_g - r_r)(r - r_r)}{l_g} + r_r\right] \tag{7}$$

where r and r^T are the original and transformed radii, respectively.

The transformation that maps the physical dimensions of the original problem onto the dimensions of the transformed problem is fully defined in Fig. 2. Based on this transformation, relationships between the field variables in the original problem and the corresponding field variables in the transformed problem can be found. In general these take the form of

$$G^T(r^T, \phi, z) = y(r)G(r, \phi, z) \tag{8}$$

where G^T represents a transformed quantity in the transformed domain, G is the corresponding quantity in the original domain and $y(r)$ defines the relationship between them. The functions represented by $y(r)$ are derived by ensuring that if G^T satisfies Maxwell's equations in the transformed domain, then G satisfies Maxwell's equations in the original domain. In other words, $y(r)$ permits the field solutions obtained in the transformed problem to be converted into the corresponding solutions to the original problem. Having derived $y(r)$ functions for all the field variables, the relationships between the material properties of the original problem and those of the transformed one can be deduced by using the constitutive relations

$$\vec{B} = \mu \vec{H} \tag{9}$$

$$\vec{J} = \sigma \vec{E} \tag{10}$$

where μ and σ are the permeability and conductivity tensors, respectively, for the unscaled regions. There is no requirement for these constitutive relations to be linear.

The technique for deriving $y(r)$ functions is now demonstrated using the magnetic flux density and magnetic flux intensity in the air gap region of an REM. Let

$$B_r^T = f_r B_r \tag{11}$$

$$B_\phi^T = f_\phi B_\phi \tag{12}$$

$$B_z^T = f_z B_z \tag{13}$$

Authorized licensed use limited to: UNIVERSITY OF SOUTHERN QUEENSLAND. Downloaded on February 25,2010 at 06:40:11 EST from IEEE Xplore. Restrictions apply.

$$H_r^T = g_r H_r \tag{14}$$

$$H_\phi^T = g_\phi H_\phi \tag{15}$$

$$H_z^T = g_z H_z \tag{16}$$

where the generic notation $y(r)$ has been replaced by the particular functions f_i and g_i for the components of $\vec{B}$ and $\vec{H}$, respectively, and i represents the subscripts r, ϕ, z. In the transformed air gap region, (1) becomes

$$\frac{1}{k_a kr}\frac{\partial(krf_r B_r)}{\partial r} + \frac{f_\phi}{kr}\frac{\partial B_\phi}{\partial \phi} + f_z\frac{\partial B_z}{\partial z} = 0 \tag{17}$$

where $k = k(r)$ and the substitution $\partial r/\partial r^T = 1/k_a$ has been made. However,

$$\frac{1}{r}\frac{\partial(rB_r)}{\partial r} + \frac{1}{r}\frac{\partial B_\phi}{\partial \phi} + \frac{\partial B_z}{\partial z} = 0 \tag{18}$$

For both (17) and (18) to hold for all r, ϕ, z it is required that:

$$\frac{B_r}{k_a k}\frac{\partial(kf_r)}{\partial r} = 0$$

and

$$\frac{f_r}{k_a} = \frac{f_\phi}{k} = f_z$$

Therefore, $f_r = c/k$ where c must be independent of r. The continuity of B_r at $r = r_r$ and B_r^T at $r^T = r_r$ imply that c must be equal to 1.

Hence,

$$f_r = \frac{1}{k} \tag{19}$$

$$f_\phi = \frac{1}{k_a} \tag{20}$$

$$f_z = \frac{1}{k_a k} \tag{21}$$

Equation (2) in the transformed air gap region expands to give

$$\frac{1}{kr}\frac{\partial(g_z H_z)}{\partial \phi} - \frac{\partial(g_\phi H_\phi)}{\partial z} = f_r J_r, \tag{22}$$

$$\frac{\partial(g_r H_r)}{\partial z} - \frac{1}{k_a}\frac{\partial(g_z H_z)}{\partial r} = f_\phi J_\phi, \tag{23}$$

$$\frac{1}{kr}\left(\frac{1}{k_a}\frac{\partial(kr\, g_\phi H_\phi)}{\partial r} - \frac{\partial(g_r H_r)}{\partial \phi}\right) = f_z J_z. \tag{24}$$

For (22)–(24) and equation (2) to hold for all r, ϕ, z it is required that

$$g_z = k g_\phi = k f_r \tag{25}$$

$$k_a g_r = g_z = k_a f_\phi \tag{26}$$

$$g_\phi = \frac{a}{k} \tag{27}$$

$$\frac{g_\phi}{k_a} = \frac{g_r}{k} = f_z \tag{28}$$

where a must be independent of r.

The current density terms in (22), (23) and (24) have not been set to zero because the transformed region is the entire region between r_r and r_g. In addition to the air gap this region may include, for example, parts of the end-shields in which currents will be induced. A further point to note is that due to the solenoidal condition of J or J^T, the relationship between these quantities is exactly the same as that between B and B^T.

Enforcing the continuity of H_ϕ at $r = r_r$ and H_ϕ^T at $r^T = r_r$, leads to a value of unity for the constant a in (27). Equations (25)–(28) inclusive are not independent. However, they are all satisfied with

$$g_r = \frac{1}{k_a} \tag{29}$$

$$g_\phi = \frac{1}{k} \tag{30}$$

$$g_z = 1 \tag{31}$$

Equations (11) through (16) can now be used to obtain the magnetic permeabilities for the transformed region. Using the constitutive relation given in (9) we have

$$\vec{B}^T = f\mu g^{-1}\vec{H}^T \tag{32}$$

where

$$f = \begin{bmatrix} f_r & 0 & 0 \\ 0 & f_\phi & 0 \\ 0 & 0 & f_z \end{bmatrix}$$

and

$$g^{-1} = \begin{bmatrix} 1/g_r & 0 & 0 \\ 0 & 1/g_\phi & 0 \\ 0 & 0 & 1/g_z \end{bmatrix}$$

Therefore the permeability tensor for the transformed region is given by

$$\mu^T = f\mu g^{-1} \tag{33}$$

For the simple case where the permeability tensor has diagonal elements only we get

$$\mu_r^T = \frac{k_a}{k}\mu_r \tag{34}$$

$$\mu_\phi^T = \frac{k}{k_a}\mu_\phi \tag{35}$$

$$\mu_z^T = \frac{\mu_z}{k_a k} \tag{36}$$

The procedures used to find the transformations for $\vec{B}, \vec{H}, \vec{J}$ and μ can also be applied to find the equivalent transformations for $\vec{E}$ and σ. An entire set of transformation rules for radial scaling have been listed in Table 1, and for axial scaling in Table 2. It should be noted that in the case of axial scaling only the air gap region is scaled. That is assuming $z = 0$ at the rotor surface:

$$\begin{aligned} z^T &= z \quad 0 \geq z \\ z^T &= k_a z \quad 0 < z < l_g \\ z^T &= z + l_g(k_a - 1) \quad l_g \geq z \end{aligned} \tag{37}$$

4 Material non-linearity

Except for the stator region in a RFM, the proposed scaling method does not involve any special procedure to account for material non-linearity. The rotor region in RFMs and both the rotor and stator regions in AFMs are unscaled. This means that material non-linearity in these regions is accounted for in the normal way. Depending on the finite element package, this requires the user to specify the constitutive relations by means of curves, or expressions representing those curves.

Authorized licensed use limited to: UNIVERSITY OF SOUTHERN QUEENSLAND. Downloaded on February 25,2010 at 06:40:11 EST from IEEE Xplore. Restrictions apply.

Table 1: Transformation rules for radial scaling

Quantity/property	Symbol	Transformation in the air gap region	Transformation in the stator region
Radial component of current density	J_r	$J_r^T = \frac{J_r}{k(r)}$	$J_r^T = \frac{J_r}{k_s}$
Angular component of current density	J_ϕ	$J_\phi^T = \frac{J_\phi}{k_a}$	$J_\phi^T = \frac{J_\phi}{k_s}$
Axial component of current density	J_z	$J_z^T = \frac{J_z}{k_a k(r)}$	$J_z^T = \frac{J_z}{k_s^2}$
Radial component of magnetic field intensity	H_r	$H_r^T = \frac{H_r}{k_a}$	$H_r^T = \frac{H_r}{k_s}$
Angular component of magnetic field intensity	H_ϕ	$H_\phi^T = \frac{H_\phi}{k(r)}$	$H_\phi^T = \frac{H_\phi}{k_s}$
Axial component of magnetic field intensity	H_z	$H_z^T = H_z$	$H_z^T = H_z$
Radial component of magnetic flux density	B_r	$B_r^T = \frac{B_r}{k(r)}$	$B_r^T = \frac{B_r}{k_s}$
Angular component of magnetic flux density	B_ϕ	$B_\phi^T = \frac{B_\phi}{k_a}$	$B_\phi^T = \frac{B_\phi}{k_s}$
Axial component of magnetic flux density	B_r	$B_z^T = \frac{B_z}{k_a k(r)}$	$B_z^T = \frac{B_z}{k_s^2}$
Radial component of electric field intensity	E_r	$E_r^T = \frac{E_r}{k_a}$	$E_r^T = \frac{E_r}{k_s}$
Angular component of electric field intensity	E_ϕ	$E_\phi^T = \frac{E_\phi}{k(r)}$	$E_\phi^T = \frac{E_\phi}{k_s}$
Axial component of electric field intensity	E_z	$E_z^T = E_z$	$E_z^T = E_z$
Radial component of permeability	μ_r	$\mu_r^T = \frac{k_a}{k(r)}\mu_r$	$\mu_r^T = \mu_r$
Angular component of permeability	μ_ϕ	$\mu_\phi^T = \frac{k(r)}{k_a}\mu_\phi$	$\mu_\phi^T = \mu_\phi$
Axial component of permeability	μ_z	$\mu_z^T = \frac{\mu_z}{k_a k(r)}$	$\mu_z^T = \frac{\mu_z}{k_s^2}$
Radial component of conductivity	σ_r	$\sigma_r^T = \frac{k_a}{k(r)}\sigma_r$	$\sigma_r^T = \sigma_r$
Angular component of conductivity	σ_ϕ	$\sigma_\phi^T = \frac{k(r)}{k_a}\sigma_\phi$	$\sigma_\phi^T = \sigma_\phi$
Axial component of conductivity	σ_z	$\sigma_z^T = \frac{\sigma_z}{k_a k(r)}$	$\sigma_z^T = \frac{\sigma_z}{k_s^2}$
Radial component of magnetic vector potential	A_r	$A_r^T = \frac{A_r}{k_a}$	$A_r^T = \frac{A_r}{k_s}$
Angular component of magnetic vector potential	A_ϕ	$A_\phi^T = \frac{A_\phi}{k(r)}$	$A_\phi^T = \frac{A_\phi}{k_s}$
Axial component of magnetic vector potential	A_z	$A_z^T = A_z$	$A_z^T = A_z$

Air is normally the only material type occupying the air-gap region of both AFMs and RFMs. Even where components such as end-shields are included in this region, it is reasonable to assume that these parts remain magnetically unsaturated. Material properties for the air-gap region are easily deduced from Table 1 or Table 2, since μ and σ in this region are independent of the field quantities.

Equation (33) applies for the stators of RFMs even if the relationship between $\vec{B}$ and $\vec{H}$ is non-linear. However, in the presence of non-linearity, μ is a function of $\vec{B}$, i.e.

$$\mu^T = f\mu\left(B_r, B_\phi, B_z\right)g^{-1} \tag{38}$$

where

$$f = \begin{bmatrix} 1/k_s & 0 & 0 \\ 0 & 1/k_s & 0 \\ 0 & 0 & 1/k_s^2 \end{bmatrix}$$

and

$$g^{-1} = \begin{bmatrix} k_s & 0 & 0 \\ 0 & k_s & 0 \\ 0 & 0 & 1 \end{bmatrix}$$

For (38) to be useful it should be expressed in terms of transformed quantities, i.e.

$$\mu^T = f\mu\left(k_s B_r, k_s B_\phi, k_s^2 B_z\right)g^{-1} \tag{39}$$

The reason this is necessary is because when a finite element analysis is performed on a scaled problem it is $\vec{B}^T$ which is calculated and not $\vec{B}$. Therefore μ^T must be expressed in terms of $\vec{B}^T$. As shown in (39), the transformation of $\mu\left(B_r, B_\phi, B_z\right)$ to $\mu\left(k_s B_r^T, k_s B_\phi^T, k_s^2 B_z^T\right)$ is performed simply by replacing B_r, B_ϕ and B_z in the expression for μ with $k_s B_r^T$, $k_s B_\phi^T$ and $k_s^2 B_z^T$, respectively.

5 Energy and power invariance

The magnetic energy stored per unit volume (W) in an unscaled region is given by

$$W = \frac{1}{2}\vec{B} \cdot \vec{H} \tag{40}$$

Authorized licensed use limited to: UNIVERSITY OF SOUTHERN QUEENSLAND. Downloaded on February 25,2010 at 06:40:11 EST from IEEE Xplore. Restrictions apply.

Table 2: Transformation rules for axial scaling

Quantity/property	Symbol	Transformation in the air gap region
Radial component of current density	J_r	$J_r^T = \frac{J_r}{k_s}$
Angular component of current density	J_ϕ	$J_\phi^T = \frac{J_\phi}{k_s}$
Axial component of current density	J_z	$J_z^T = J_z$
Radial component of magnetic field intensity	H_r	$H_r^T = H_r$
Angular component of magnetic field intensity	H_ϕ	$H_\phi^T = H_\phi$
Axial component of magnetic field intensity	H_z	$H_z^T = \frac{H_z}{k_s}$
Radial component of magnetic flux density	B_r	$B_r^T = \frac{B_r}{k_s}$
Angular component of magnetic flux density	B_ϕ	$B_\phi^T = \frac{B_\phi}{k_s}$
Axial component of magnetic flux density	B_z	$B_z^T = B_z$
Radial component of electric field intensity	E_r	$E_r^T = E_r$
Angular component of electric field intensity	E_ϕ	$E_\phi^T = E_\phi$
Axial component of electric field intensity	E_z	$E_z^T = \frac{E_z}{k_s}$
Radial component of permeability	μ_r	$\mu_r^T = \frac{\mu_r}{k_s}$
Angular component of permeability	μ_ϕ	$\mu_\phi^T = \frac{\mu_\phi}{k_s}$
Axial component of permeability	μ_z	$\mu_z^T = k_s \mu_z$
Radial component of conductivity	σ_r	$\sigma_r^T = \frac{\sigma_r}{k_s}$
Angular component of conductivity	σ_ϕ	$\sigma_\phi^T = \frac{\sigma_\phi}{k_s}$
Axial component of conductivity	σ_z	$\sigma_z^T = k_s \sigma_z$
Radial component of magnetic vector potential	A_r	$A_r^T = A_r$
Angular component of magnetic vector potential	A_ϕ	$A_\phi^T = A_\phi$
Axial component of magnetic vector potential	A_z	$A_z^T = \frac{A_z}{k_s}$

and in the corresponding scaled region

$$W^T = \frac{1}{2}\vec{B}^T \cdot \vec{H}^T = \frac{1}{2}\left(f_r g_r B_r H_r + f_\phi g_\phi B_\phi H_\phi + f_z g_z B_z H_z\right) \quad (41)$$

Inspection of Tables 1 and 2 shows that irrespective of the scaled region it is always true that

$$f_r g_r = f_\phi g_\phi = f_z g_z \quad (42)$$

Therefore,

$$W^T = f_z g_z W \quad (43)$$

It can also be shown that elemental volume elements in scaled and unscaled regions are always related by

$$dV^T = \frac{dV}{f_z g_z} \quad (44)$$

It is concluded from (43) and (44) that the magnetic energy stored in a scaled region is identical to that stored in the corresponding unscaled region. This result is also true for ohmic power dissipation per unit volume $\left(\vec{E} \cdot \vec{J}\right)$. The magnetic energy or power invariance property greatly simplifies post processing as there is no need to transform the these quantities. Invariance in magnetic energy implies that torque and inductance are also invariant. Total power loss due to induced currents will also be invariant under the transformation.

6 Practical implementation

It may seem, particularly in cases where there are regions in which the field variables change rapidly in space, that the coarser mesh produced by the scaling process will result in increased solution errors. However, if adaptive meshing methods are used this will not be the case. Even where adaptive meshing is not available, manually controlled mesh refinement can be used to improve solution accuracy. The reduction in the number of nodes due to the scaling process will be problem dependant. At one extreme, scaling a problem which has an already large air gap region may not produce any benefit. On the other hand there will be instances where, due to very poor aspect ratios in the geometry, an acceptable finite element solution may not be possible without the use of some form of scaling. An excessively small air gap may even cause generic meshing algorithms to fail or produce poor quality meshes.

The scaling technique has been applied to a switched reluctance motor test problem [13]. All relevant details are given in Figs. 3 and 4. Results from the finite element analysis are given in Tables 3–5 and Figs. 5–8. It was performed in FEMLAB® using tetrahedral (3-D) and triangular (2-D) edge elements based on the magnetic vector potential formulation [14]. The aim is to demonstrate that field quantities (Figs. 5 and 6) and other quantities such as the magnetic energy (Figs. 7 and 8) for the unscaled problem are derivable from the corresponding quantities

Authorized licensed use limited to: UNIVERSITY OF SOUTHERN QUEENSLAND. Downloaded on February 25,2010 at 06:40:11 EST from IEEE Xplore. Restrictions apply.

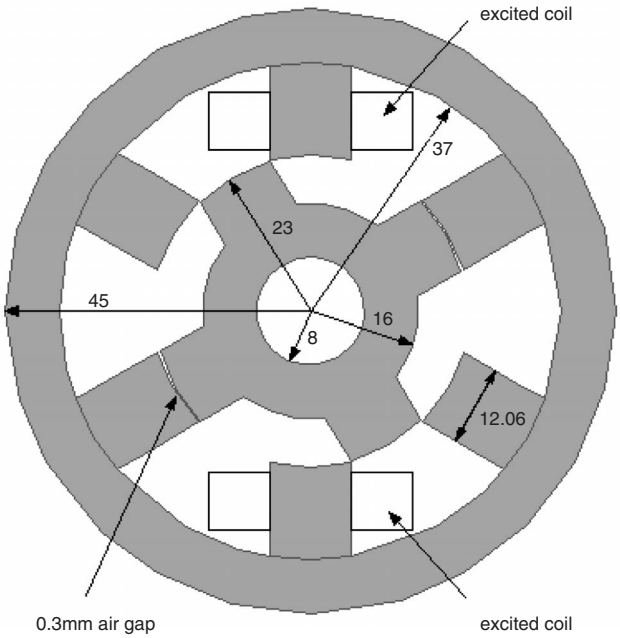

Fig. 3 *Switched Reluctance Motor configuration and dimensions (in mm)*

Table 3: Finite Element results for test case presented in Fig. 3 with adaptive meshing not used

FEM Model	Rotor angle	Scale factor	Degrees of freedom	Number of elements	Solution time, s
2-D	0	1	12068	5998	29.94
2-D	0	5	4944	2436	4.08
2-D	5	1	12148	6038	5.31
2-D	5	5	4936	2432	2.11
2-D	10	1	12169	6062	5.36
2-D	10	5	4932	2430	2.14
2-D	15	1	24696	12320	10.01
2-D	15	5	4908	2430	3.94
2-D	20	1	12008	5968	3.41
2-D	20	5	4916	2422	1.72
2-D	25	1	12732	6330	4.47
2-D	25	5	4896	2412	1.67
2-D	30	1	12212	6070	2.38
2-D	30	5	4976	2452	1.22
2-D	35	1	12192	6060	2.44
2-D	35	5	5000	2464	1.22
2-D	40	1	12352	6140	2.31
2-D	40	5	4976	2452	1.27
2-D	45	1	24992	12468	6.23
2-D	45	5	4132	2038	1.09

obtained from the scaled problem. Magnetic energy was chosen as a comparison value because practical quantities such as stator flux linkage and torque are obtainable directly from it or from its angular derivative.

Table 3 shows that there is a considerable reduction (greater than 60%) in the number of elements required when scaling is used with non-adaptive meshing. Solution times are also reduced by more than 50%. There is good agreement between magnetic energies obtained for the scaled and unscaled problems as shown in Fig. 7. Considerably

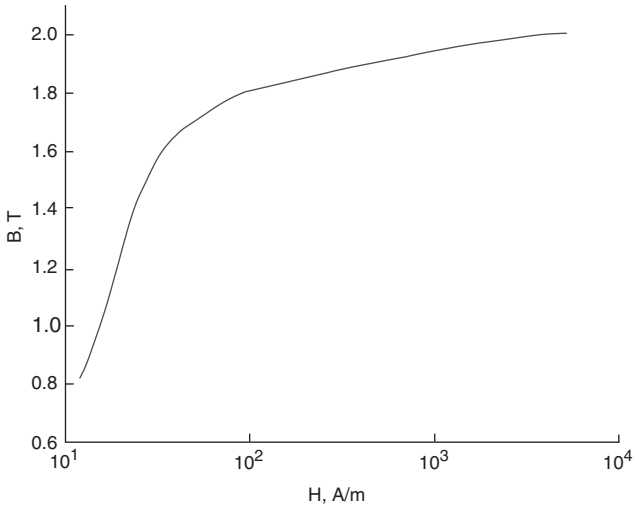

Fig. 4 *Stator and rotor iron magnetisation curve*

Table 4: Finite element results for test case presented in Fig. 3 with adaptive meshing used

FEM model	Rotor angle	Scale factor	Degrees of freedom	Number of elements	Solution time, s
2-D	0	1	17424	8676	48.53
2-D	0	5	11492	5710	15.55
2-D	5	1	12288	6108	16.14
2-D	5	5	10220	5074	8.38
2-D	10	1	12316	6122	9.42
2-D	10	5	10004	4966	5.95
2-D	15	1	24712	12328	20.41
2-D	15	5	10207	5079	10.58
2-D	20	1	12104	6016	7.13
2-D	20	5	10488	5208	5.72
2-D	25	1	13496	6712	15.0
2-D	25	5	10820	5374	7.38
2-D	30	1	17188	8558	6.44
2-D	30	5	11220	5574	4.56
2-D	35	1	17304	8616	6.64
2-D	35	5	10388	5158	4.17
2-D	40	1	17475	8701	6.74
2-D	40	5	10808	5368	4.83
2-D	45	1	33793	16867	19.81
2-D	45	5	9163	4553	3.75

Table 5: Three-dimensional finite element results for the test case presented in Fig. 3

FEM model	Rotor angle	Scale factor	Degrees of freedom	Number of elements	Magnetic energy, J/m
3-D	0	1	517599	120573	Unable to solve
3-D	0	5	183738	40467	2.0011
2-D	0	1	12068	5998	2.0201

better agreement in magnetic energies is obtained if adaptive meshing is used. However, the savings in the number of elements, although still significant, are not as great.

Authorized licensed use limited to: UNIVERSITY OF SOUTHERN QUEENSLAND. Downloaded on February 25,2010 at 06:40:11 EST from IEEE Xplore. Restrictions apply.

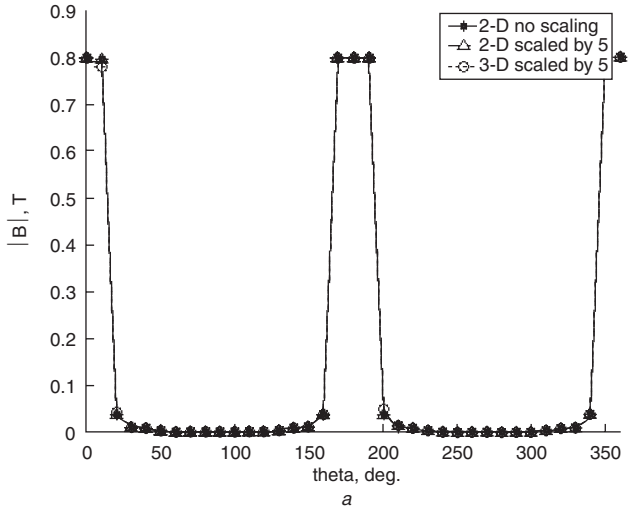

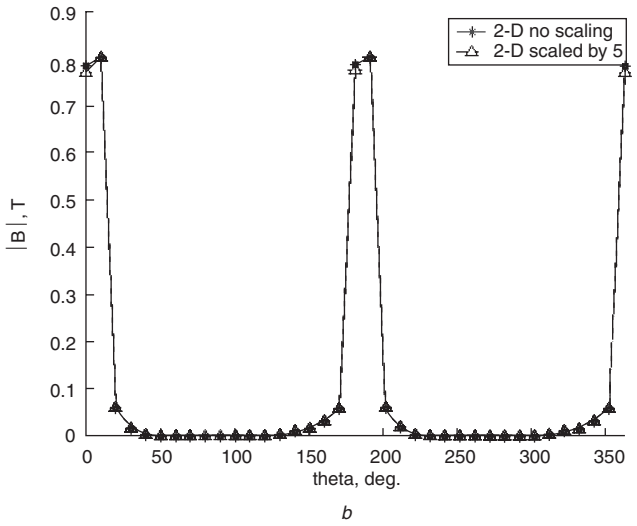

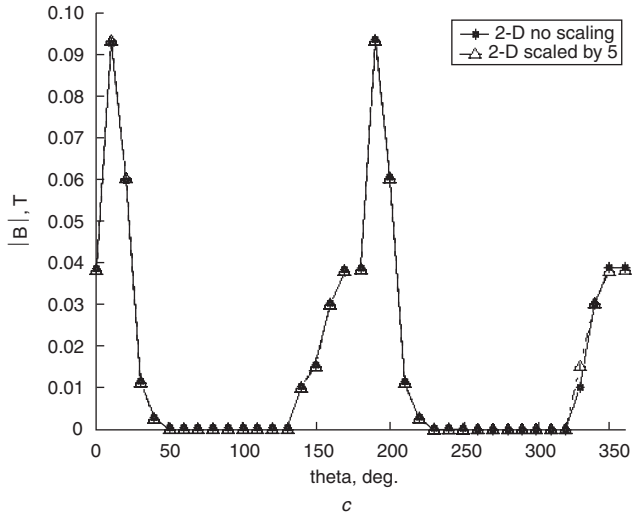

Fig. 5 *Mid-air-gap magnetic flux density |B| (finite element analysis using adaptive meshing)*
a with poles aligned
b with poles 15 degrees from alignment
c with poles 30 degrees from alignment

Figure 5 provides comparisons between the flux densities in the air gap for the scaled and unscaled problems. Discrepancies are practically negligible. Figure 6 illustrates that agreement is reasonable in non-linear stator regions.

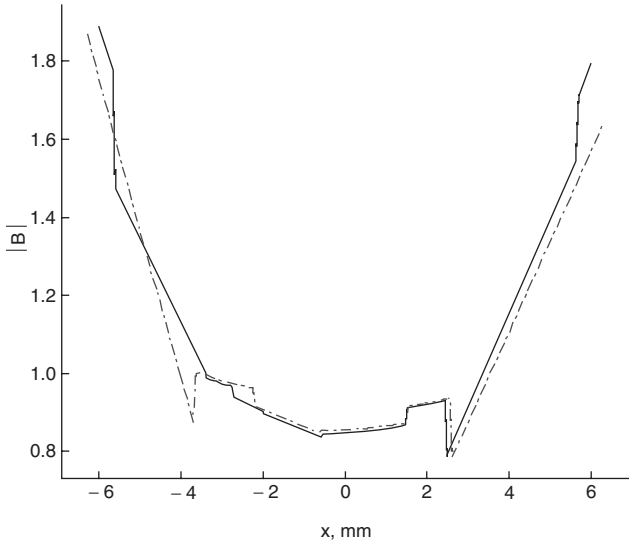

Fig. 6 *|B| at the root of one of excited stator poles (rotor angle = 0 degrees)*

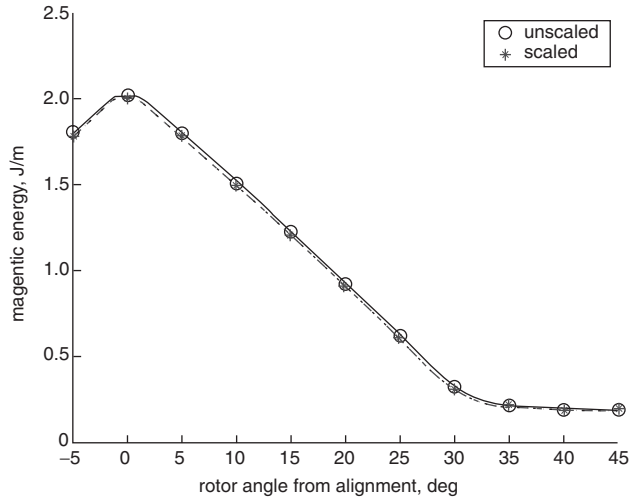

Fig. 7 *Magnetic energy against rotor position (FEA with non-adaptive meshing)*

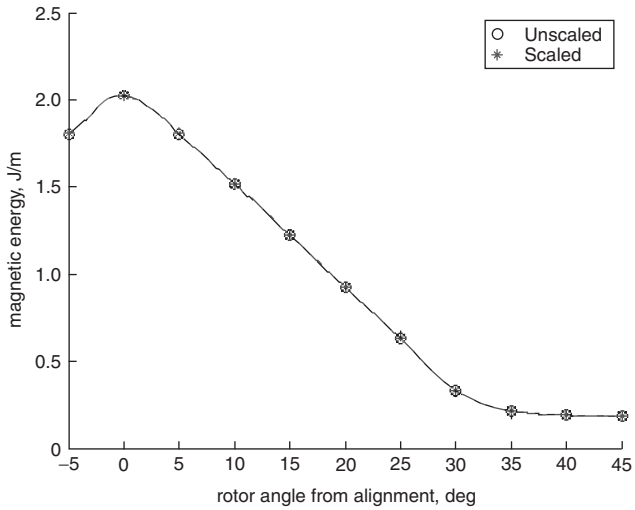

Fig. 8 *Magnetic energy against rotor position (FEA adaptive meshing)*

The 3-D results given in Table 5 are also for the machine described in Figs. 3 and 4. End effects have been ignored to permit comparison with the 2-D models. Poor aspect ratios, especially in 3-D problems, can result in such a large

Authorized licensed use limited to: UNIVERSITY OF SOUTHERN QUEENSLAND. Downloaded on February 25,2010 at 06:40:11 EST from IEEE Xplore. Restrictions apply.

number of elements that a solution cannot be calculated with available computing resources. The results given in Table 5 demonstrate that the scaling technique has the potential to rectify this problem.

7 Conclusions

The scaling techniques presented here have been developed to allow more efficient meshing for finite element analysis of electrical machines with relatively thin air gaps. Two sets of transformation equations have been presented, one for the scaling of the air gap of radial flux machines and the other for axial flux machines. The transformation equations allow a machine with a relatively thin air gap to have its geometry transformed into one which can be analysed with a significant reduction in the number of elements. These equations also allow the field solutions to the scaled problem to be simply converted into solutions to the original problem. Since no simplifying assumptions have been made in the development of the transformation equations, the proposed scaling techniques are potentially useful for all low frequency electromagnetic problems. In the case of axial flux machines, a major advantage of the proposed scaling method is that it can be implemented using any finite element package. To apply the method to radial flux machines, the finite element software should support position dependence for material properties. The scaling process involves only simple manipulation of data during the pre- and post- processing stages of an analysis.

8 References

1 Lipo, T. (ed.): 'Finite element analysis of electrical machines' (Kluwer Academic Publishers, 1995)
2 Binns, B.J., Lawrenson, P.J., and Trowbridge, C.W.: 'The analytical and numerical solution of electric and magnetic fields' (Wiley & Sons, 1992)
3 Guerin, C., Tanneau, G., Meunier, G., Brunotte, X., and Albertini, J.: 'Three dimensional magnetoststic finite elements for gaps and iron shells using magnetic scalar potentials', *IEEE Trans. Magn.*, 1994, **30**, (5), pp. 2885–2888
4 Abdel-Razek, A.A., Coulomb, J.L., Feliachi, M., and Sabonnadiere, J.C.: 'Conception of an air-gap element for the dynamic analysis of the electromagnetic field in electric machines', *IEEE Trans. Magn.*, 1982, **MAG-18**, (2), pp. 655–659
5 Feliachi, M., Coulomb, J.L., and Mansir, H.: 'Second order air-gap element for the dynamic finite-element analysis of the electromagnetic field in electric machines', *IEEE Trans. Magn.*, 1983, **MAG-19**, (6), pp. 2300–2303
6 DeBortoli, M.J., Lee, M.J., Salon, S.J., and Lee, K.: 'Coupling finite elements and analytical solution in the airgap of electrical machines', *IEEE Trans. Magn.*, 1991, **27**, (5), pp. 3955–3957
7 Melissen, J.B.M., and Simkin, J.: 'A new coordinate transform for the finite element solution in magnetostatics', *IEEE Trans. Magn.*, 1990, **26**, (2), pp. 391–394
8 Ouazzani, W.E., Rioux-Damidau, F., Brunotte, X., and Meunier, G.: 'Finite element modelling of unbounded problems: use of geometrical transformation and comparison with boundary integral method', *IEEE Trans. Magn.*, 1999, **32**, (3), pp. 1401–1404
9 Henrotte, F., Meys, B., Hedia, H., Dular, P., and Legros, W.: 'Finite element modelling with transformation techniques', *IEEE Trans. Magn.*, 1999, **35**, (3), pp. 1434–1437
10 Choi, H.S., Kim, D.H., Park, I.H., and Hahn, S.Y.: 'A new design technique of magnetic systems using space mapping algorithm', *IEEE Trans. Magn.*, 2001, **37**, (5), pp. 3627–3630
11 Adams, V., and Askenazi, A.: 'Building better products with finite element analysis', (OnWord Press, 1999)
12 Logan, D.L.: 'A first course in the finite element method' (Brooks/Cole, 2002)
13 Reece, A.B.J., and Preston, T.W.: 'Finite element methods in electrical power engineering', (Oxford University Press, 2000)
14 FEMLAB, Electromagnetics module users guide, Version 3.0, COMSOL AB, http://www.comsol.com, (last accessed June 2004)

Authorized licensed use limited to: UNIVERSITY OF SOUTHERN QUEENSLAND. Downloaded on February 25,2010 at 06:40:11 EST from IEEE Xplore. Restrictions apply.